

<https://doi.org/10.1038/s44298-025-00113-0>

Genetic diversity of Toscana virus glycoproteins affects the kinetics of virus entry and the infectivity of newly produced virions

Check for updates

Adrien Thiesson¹, Marie-Pierre Confort¹, Sophie Desloire¹, Alain Kohl^{2,3}, Frédérick Arnaud¹ ✉ & Maxime Ratnier¹ ✉

Toscana virus (TOSV) is a pathogenic and transmissible *Phlebovirus* of the *Bunyavirales* order. To date, two principal genetic lineages (A and B) have been identified and the impact of TOSV genetic diversity on its biology is still unknown. We used a reverse genetic approach based on two TOSV strains belonging to lineage A or B (i.e., TOSV-A and TOSV-B) and displaying different in vitro replicative fitness. Our results demonstrate that the sequences of Gn and Gc glycoproteins are responsible for the differences in replicative fitness between the two TOSV strains. Moreover, our data show that TOSV-A and TOSV-B display different entry kinetics and that newly-produced virions have different infectivity. This comparative approach demonstrates that the genetic diversity of TOSV can significantly impact viral properties and highlights the need for better molecular characterisation of the genomes of circulating TOSV strains, with a particular focus on the viral Gn and Gc glycoproteins.

Toscana virus (TOSV) is an arbovirus of the *Bunyavirales* order and the *Phenuiviridae* family. It is transmitted by sand flies, mostly *Phlebotomus perniciosus* and *P. perfiliewi*¹. Isolated for the first time in Italy in 1971², TOSV is now found in 23 different countries around the Mediterranean basin^{3–5}. Infection in humans is generally asymptomatic or leads to mild symptoms⁶ but can progress to severe neurological disease following viral invasion of the central nervous system (CNS)^{7,8}. TOSV is now considered as one of the leading causes of meningitis and encephalitis in humans during summer⁹.

Two main distinct TOSV genetic lineages have been identified thus far based on phylogenetic analyses, and referred to as lineages A and B¹⁰. More recently, a third lineage (referred to as lineage C) was described based on partial viral sequences; however, this virus has not been isolated so far^{11,12}. While lineage A and B strains were historically described in Italy and Spain, respectively, recent studies have shown that their geographic distribution is broader, spanning from the eastern to the western Mediterranean basin⁹. Lineage C appears to be restricted to Greece and the Balkan region; however, this conclusion is based on limited evidence. The specific factors contributing to the geographic distribution and diversity of TOSV remain to be determined.

Despite the significant impact of TOSV on human health as an emerging cause of CNS infections, this virus remains an understudied pathogen. For instance, the impact of TOSV genetic diversity on viral pathogenicity is still unknown. Yet this represents an important point to address to understand TOSV disease and design preventive measures. Recently, we and others have developed reverse genetic systems for TOSV that allow manipulation of the viral genome^{13,14}, providing new opportunities to investigate TOSV molecular biology.

In this study, two TOSV strains from lineages A (TOSV-A) and B (TOSV-B) were studied using reverse genetic approaches and reassortant viruses. Our results demonstrate that TOSV-A replicates at a higher rate than TOSV-B, due to differences in Gn and Gc coding sequences. In addition, our data show that TOSV-A and TOSV-B display different entry kinetics and that newly produced virions have different infectivity. Overall, our results highlight the significant impact of the genetic diversity of the glycoproteins of TOSV strains on virus biological characteristics. This points to the urgent need for more and wider molecular characterisation of circulating TOSV strains for a better understanding of this pathogen.

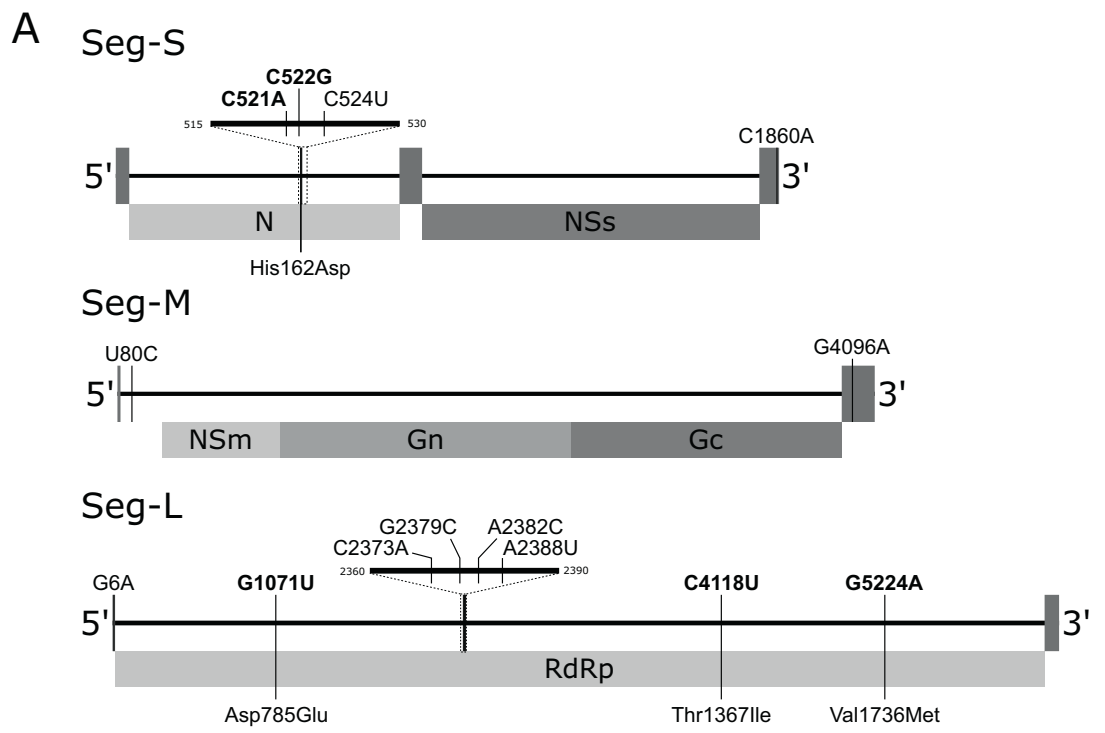
¹IVPC UMR754, INRAE, Université Claude Bernard Lyon 1, EPHE, Université PSL, Lyon, France. ²MRC-University of Glasgow Centre for Virus Research, Glasgow, UK. ³Centre for Neglected Tropical Diseases, Departments of Tropical Disease Biology and Vector Biology, Liverpool School of Tropical Medicine, Liverpool, UK. ✉e-mail: frederick.arnaud@univ-lyon1.fr; maxime.ratnier@univ-lyon1.fr

Results

Development of a reverse genetic system for TOSV-B

We previously published a reverse genetic system for one strain of TOSV lineage A TOSV (TOSV 1500590, referred to as wild-type [wt] TOSV-A)^{13,15}. Here, we developed a reverse genetic system for one strain of TOSV lineage B (TOSV MRS2010-4319501, referred to as wt TOSV-B)¹⁶. To this end, the three antigenomic segments (Seg-S, Seg-M, and Seg-L) of the wt TOSV-B were amplified by RT-PCR and cloned into reverse genetic plasmids. Next, the sequences from these plasmids were compared to those of the wt TOSV-B strain reference genome available on GenBank¹⁶. Several substitutions were identified in all the segments: three in Seg-S, two in Seg-M, and seven in Seg-L (Fig. 1A). The three substitutions in the Seg-S are in the coding sequence of the N protein: C521A and C522G, both resulting into a change of amino acid (His162Asp), and C524U (silent substitution). The two substitutions in the Seg-M are in the anti-genomic untranslated regions (UTRs): U80C, in the 5' UTR, and G4096A, in the 3' UTR. Finally, the seven substitutions in Seg-L are in the L polymerase

coding sequence: G1071U (Asp785Glu), C2373A, G2379C, A2382C, A2388U, C4118U (Thr1367Ile), and G5224A (Val1736Met). To ensure that these substitutions were not generated during TOSV genome amplification, segments were again amplified by RT-PCR from wt TOSV B and re-sequenced. This confirmed that the cloned sequences were correct. Furthermore, these sequences were compared to those of other TOSV strains belonging to lineage B and available on GenBank. As shown in Fig. 1B, these sequences are identical, except for substitution U80C in the anti-genomic 5' UTR. Thus, the 5' UTR and 3' UTRs of each segment from our viral stock were re-sequenced by RACE PCR, confirming the U80C substitution in the wt TOSV-B antigenome. In addition, when comparing the results from the RACE-PCR and the sequences of the TOSV-B plasmids, two additional nucleotide substitutions were identified: one in the Seg-S 3' UTR (C1860A), and the other one in the Seg-L 5' UTR (G6A). These 2 substitutions were modified by site-directed mutagenesis to correct the sequence of the two plasmids containing the Seg-S and Seg-L for reverse genetics purposes.



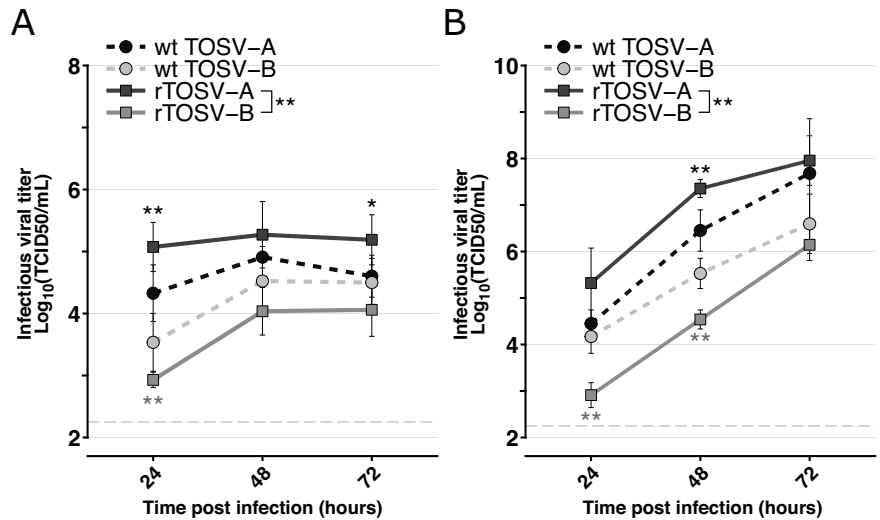
B

	L								M		S			
	6	1071	2373	2379	2382	2388	4118	5224	80	4096	521	522	524	1860
RG plasmid	A	U	A	C	C	U	U	A	C	A	A	G	U	A
MRS2010-4319501	G	G	C	G	A	A	C	G	U	G	C	C	C	C
TOSV/P51	U
9028	U
11368	U
TOSV-54441132704	U
P233	U
H4906	U
5963930705	G	U
Nice/113	U	-

Fig. 1 | Comparison between the sequences of TOSV-B reverse genetic plasmids and those of TOSV lineage B reference genomes. A Schematic representation of the TOSV antigenome segments: Seg-S, Seg-M, and Seg-L. The location of the viral 5' and 3' untranslated regions (UTR) and open reading frame of the structural (N, Gn, Gc and RNA-dependent RNA polymerase [RdRp]) and non-structural (NSs and NSm) viral proteins are indicated. The 14 substitutions identified between the reference sequences of the wt TOSV-B and those of the plasmid developed for the

reverse genetics system (indicated as RG plasmid) are presented. Non-synonymous substitutions are in bold and their respective change in amino acid is indicated. **B** Nucleotide differences between TOSV-B strains. Sequences were aligned using MUSCLE software. Dots indicate identical nucleotides. Note that, for Nice/113 strain, Seg-S sequence is incomplete at the 3' UTR, thereby preventing comparison at position 1860.

Fig. 2 | TOSV-A viruses produce higher infectious titers than TOSV-B. Growth curves of wt TOSV-A, wt TOSV-B, rTOSV-A and rTOSV-B in A549 (A) or A549 Npro (B) cells (MOI = 0.01). Cell supernatants were collected at 24-, 48-, and 72-hours post-infection, and viral titers were obtained by TCID50 limiting-dilution assays in A549V cells. Each experiment was performed in triplicate and at least three times independently. Bars indicate standard deviations. Light grey dashed lines indicate the threshold of virus detection [2.25 Log₁₀(TCID50/mL)]. Statistical significance was determined using multiple Wilcoxon tests with the Benjamini-Yekutieli (BY) *p*-value adjustment method: *p* < 0.05 (*) and *p* < 0.01 (**). Black and grey stars indicate the statistical significance of the rescued viruses compared to their parental virus strain (i.e., wt TOSV-A or wt TOSV-B, respectively).



rTOSV-A replicates more than rTOSV-B

The replication rates of TOSV-A and TOSV-B rescued viruses (hereafter referred to as rTOSV-A and rTOSV-B) were compared to those of their parental virus strains (i.e., wt TOSV-A and wt TOSV-B) in A549 and A549 Npro cells. A549 Npro cells constitutively express the N-terminal protease of bovine viral diarrhea virus, which blocks type I interferon (IFN-I) synthesis¹⁷, thus allowing to assess the impact of IFN-I responses on TOSV replication. The infectious virus production by rTOSV-A, rTOSV-B, wt TOSV-A, and wt TOSV-B was determined by TCID50 assays from the supernatants of infected cells (Fig. 2). Unlike rTOSV-B, rTOSV-A had higher viral titers than wt TOSV-A in both A549 and A549 Npro cells (Fig. 2). Importantly, both rTOSV-B and wt TOSV-B produced lower viral titers than rTOSV-A and wt TOSV-A in both cell lines. Overall, these data indicate that rescued viruses behave similarly to their respective parental virus strains, and suggest that the difference observed between TOSV-A and TOSV-B does not depend on the IFN-I pathway.

Seg-M modulates TOSV replication in vitro

The comparative genomic analyses of rTOSV-A and rTOSV-B revealed a high genetic diversity across the TOSV genome. In order to assess which of the three TOSV segments is responsible for the viral titer differences observed, a library of reassortant viruses was generated for each of the three genome segments, and their respective replication rates were assessed in A549 and A549 Npro cells (Fig. 3A, B). Seg-L and Seg-S reassortant viruses had similar viral titers to those of their corresponding parental viruses (i.e., rTOSV-A or rTOSV-B) in both cell lines. However, rTOSV-A-MB (a reassortant virus carrying the Seg-S and Seg-L of TOSV-A and the Seg-M of TOSV-B) produced significantly lower viral titers than rTOSV-A (*p*-value < 0.05 in A549 cells; *p*-value < 0.01 in A549 Npro cells). Conversely, rTOSV-B-MA (a reassortant virus carrying the Seg-S and Seg-L of TOSV-B and the Seg-M of TOSV-A) had significantly higher viral titers than rTOSV-B (*p*-value < 0.05 in A549 cells; *p*-value < 0.01 in A549 Npro cells). These data demonstrate that Seg-M carries the viral determinant responsible for the higher replication rate of rTOSV-A compared to rTOSV-B.

The Gn-Gc coding sequence modulates TOSV replication

TOSV Seg-M encodes a polyprotein which is further cleaved by the host proteases into NSm, Gn, and Gc¹⁸. Genomic comparison between rTOSV-A and rTOSV-B showed a high genetic diversity distributed throughout the entire M polyprotein coding sequence (Fig. 4A). Interestingly, the NSm harbours a higher genetic diversity (81% amino acid strictly identical) compared to the Gn or Gc (89% and 95%, respectively). In order to understand which of these proteins is involved in modulating TOSV replication rate, chimeric Seg-M were produced by exchanging NSm or Gn

Gc coding sequence between rTOSV-A and rTOSV-B (Fig. 4A). The replication rates of these rescued viruses were assessed in A549 Npro cells (Fig. 4B–D). No significant difference was observed in the replication kinetics of the two NSm chimeric viruses (Fig. 4B). However, rTOSV-A-GnGcB displayed significantly lower viral titers than rTOSV-A (*p*-value < 0.01; Fig. 4C). Conversely, rTOSV-B-GnGcA showed significantly higher viral titers than rTOSV-B (*p*-value < 0.002; Fig. 4D). Altogether, these data demonstrated that the Gn-Gc coding sequence is responsible for the higher replication rate of rTOSV-A compared to rTOSV-B.

rTOSV-A virions are internalised faster than rTOSV-B in infected cells

Phlebovirus glycoproteins play a key role in virus entry¹⁹. In order to understand whether the genetic diversity within the Gn-Gc coding sequence of rTOSV-A and rTOSV-B could affect the viral entry process, a virus penetration kinetic assay was carried out as described in Fig. 5A. Data were analysed using a 3-parameter logistic model described elsewhere²⁰. Cell internalization of rTOSV-A started within the first 10 min following temperature shift, and it increased over time to reach the half-maximal level (t1/2) within 22.84 ± 1.19 min, and a plateau 20 min later (Fig. 5B). In contrast, rTOSV-B reached the t1/2 in 34.88 ± 1.34 min (Fig. 5B). These data demonstrate that the cell penetration kinetic of rTOSV-A occurs faster than that of rTOSV-B.

rTOSV-B Gn-Gc are more abundant than rTOSV-A Gn-Gc in infected cell supernatants

The rTOSV-A and rTOSV-B Gn and Gc expression and properties were further characterized by western blot. As shown in Fig. 6A, rTOSV-B Gc molecular weight is approximately 0.9 kDa lower than that of rTOSV-A. To investigate if this difference was due to the different N-glycosylation patterns of rTOSV-A and rTOSV-B Gc proteins, rTOSV-A and rTOSV-B virions from A549 Npro infected cells were treated with PNGase-F. No difference in terms of glycosylation between rTOSV-A and rTOSV-B Gc proteins was observed (Fig S1). In addition, rTOSV-A and rTOSV-B infected cells had similar Gn and N protein levels (Figs. 6A, B). However, rTOSV-B infected cells had significantly higher Gc levels compared to rTOSV-A infected cells (*p*-value < 0.0001; Fig. 6B). Moreover, higher Gn and Gc levels were found in the supernatants of rTOSV-B infected cells compared to rTOSV-A infected cells (Fig. 6A, B), suggesting a higher incorporation of Gn and Gc into newly produced rTOSV-B virions.

The intracellular localisation of rTOSV-A and rTOSV-B Gn and Gc proteins was also investigated in A549 Npro cells. Both proteins displayed a perinuclear localisation, potentially reflecting localisation in the endoplasmic reticulum and/or Golgi apparatus (Fig S2).

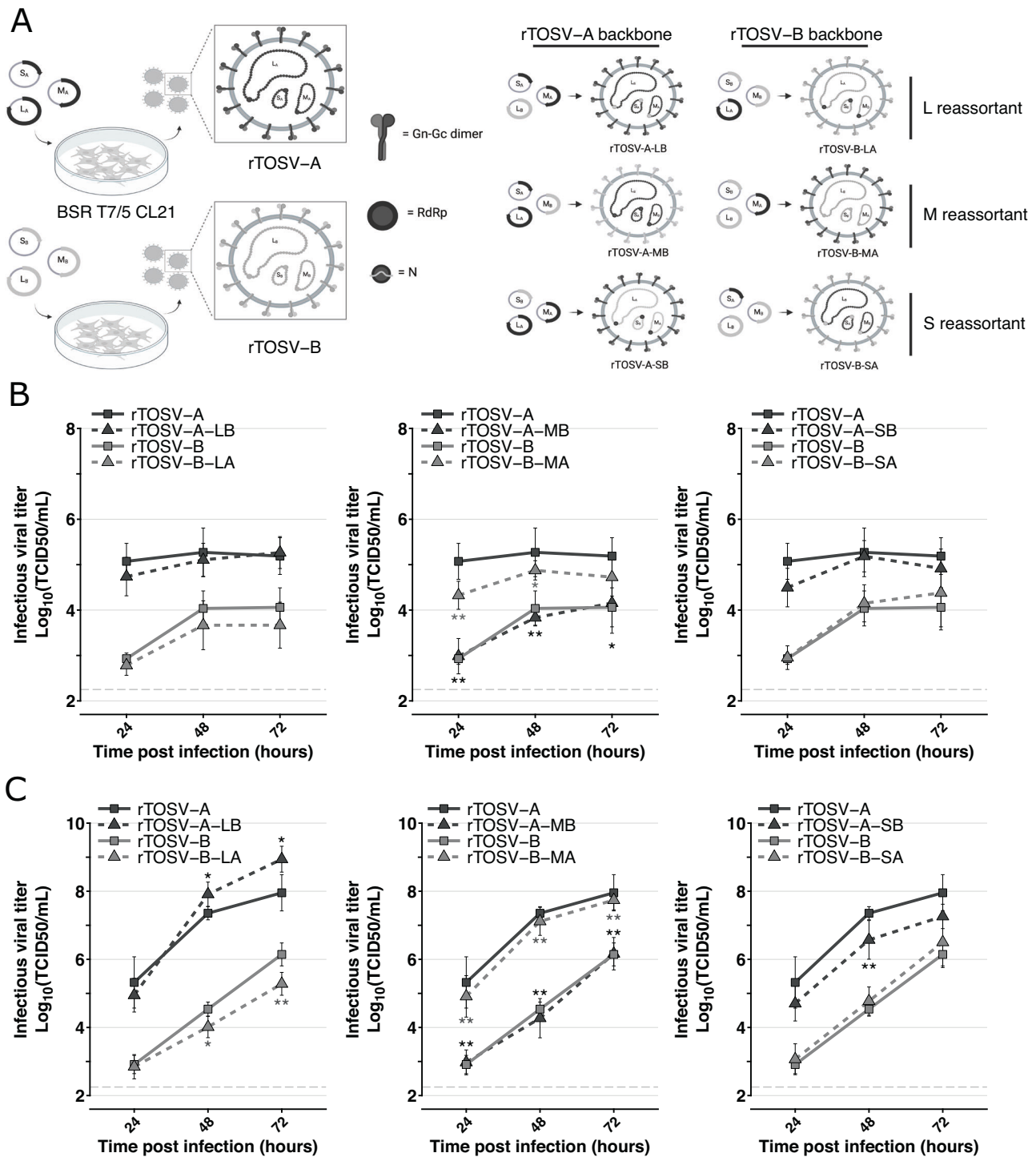


Fig. 3 | Seg-M modulates TOSV replication rates in A549 and A549 Npro cells. A Schematic representation of the reverse genetic system and the reassortant viruses produced. Figure panel created with BioRender. THIESSON, A. (2025) <https://BioRender.com/z67g107>. Growth curves of rTOSV-A and rTOSV-B and their respective Seg-L (LB or LA), Seg-M (MB or MA) and Seg-S (SB or SA) reassortant viruses in A549 (B) or A549 Npro (C) cells (MOI = 0.01). Cell supernatants were collected at 24-, 48-, and 72 h post-infection, and viral titers were determined by TCID₅₀ limiting-dilution assays in A549V cells. Each experiment was performed in

triplicate and at least three times independently. Bars indicate standard deviations. Light grey dashed lines indicate the threshold of virus detection [2.25 Log₁₀(TCID₅₀/mL)]. Statistical significance was determined using multiple Wilcoxon tests with the BY *p*-value adjustment method: *p* < 0.05 (*) and *p* < 0.01 (**). Black and grey stars indicate the statistical significance of reassortant viruses compared to their corresponding parental virus (i.e., rTOSV-A or rTOSV-B, respectively).

Newly produced rTOSV-A virions display a higher infectivity than rTOSV-B

In order to understand if the increased amount of Gn and Gc proteins incorporated into newly produced rTOSV-B virions could affect viral

infectivity, physical and infectious titers of both rTOSV-A and rTOSV-B were determined in the supernatants of infected cells before the appearance of cytopathic effects. To this end, the number of rTOSV-A and rTOSV-B genomic copies was quantified by RT-qPCR, and the number of infectious

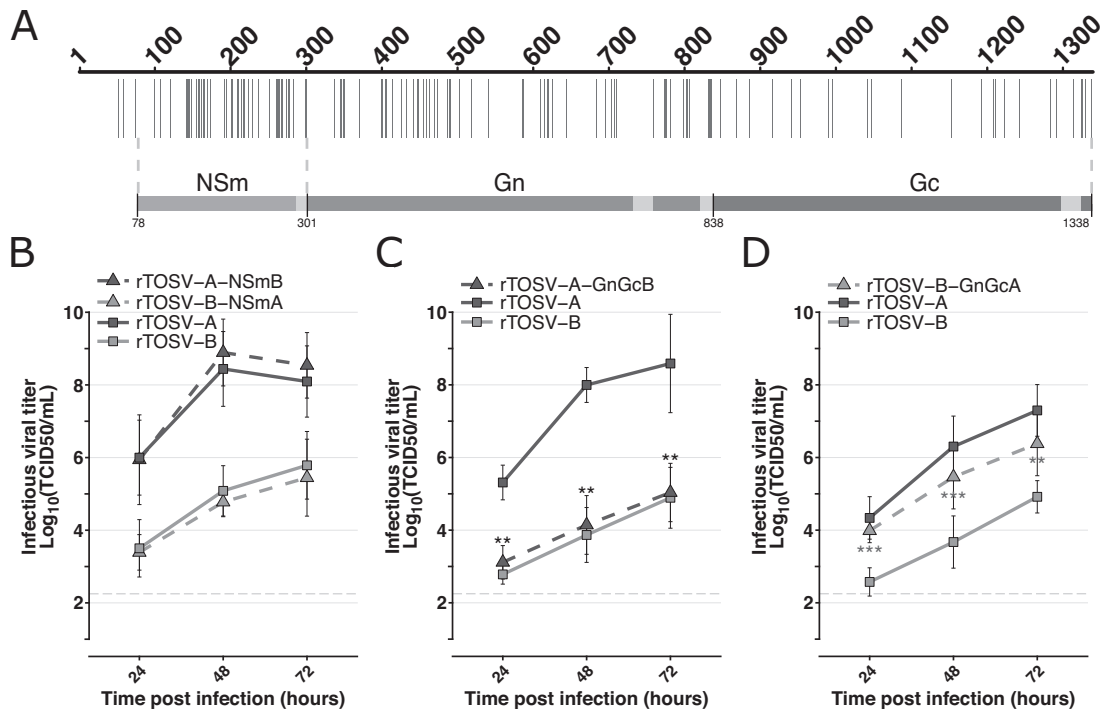


Fig. 4 | Gn-Gc modulates TOSV replication rates in A549 Npro cells. **A** Schematic representation of the M polyprotein sequence alignment between rTOSV-A and rTOSV-B. Each vertical bar represents an amino acid substitution. The region corresponding to either NSm or Gn-Gc protein is indicated. Light grey regions indicate transmembrane domains. The dashed lines show the limits of the exchanged coding sequence in the NSm or Gn-Gc chimeric viruses. **B–D** Growth curves in A549 Npro cells infected with rTOSV-A, rTOSV-B or NSm (**B**), rTOSV-A-GnGcB (**C**), or rTOSV-B-GnGcA (**D**) chimeric viruses (MOI = 0.01). Cell supernatants were

collected at 24-, 48-, and 72-hours post-infection, and viral titers were obtained by TCID₅₀ limiting-dilution assays in A549V cells. Each experiment was performed in triplicate and at least three times independently. Bars indicate standard deviations. Light grey dashed lines indicate the threshold of virus detection [2.25 Log₁₀(TCID₅₀/mL)]. Statistical significance was determined using multiple Wilcoxon tests with the BY p-value adjustment method: $p < 0.05$ (*) and $p < 0.01$ (**). Black and grey stars indicate the statistical significance of chimeric viruses compared to their corresponding parental virus (i.e., rTOSV-A or rTOSV-B, respectively).

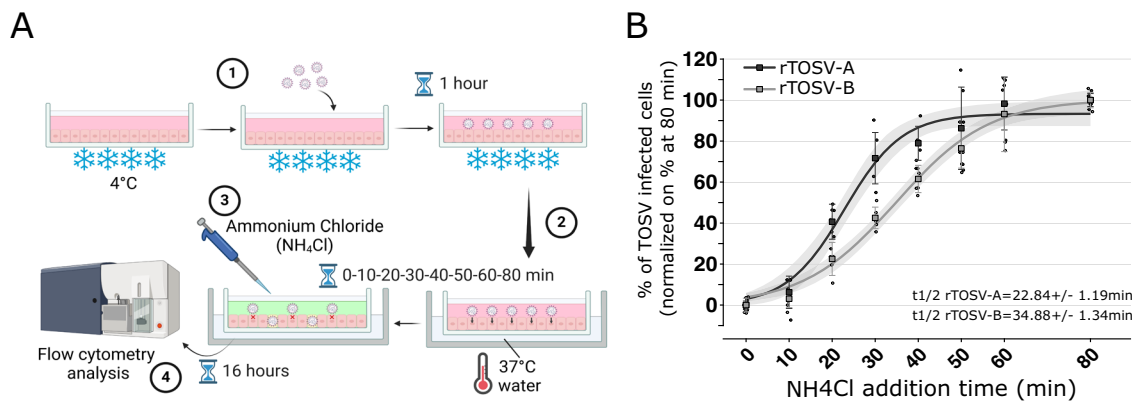


Fig. 5 | rTOSV-A virions are internalized faster than rTOSV-B virions. **A** Schematic representation of the penetration kinetic workflow used in this study. rTOSV-A and rTOSV-B virions were bound on A549 Npro cells at MOI = 1 (1). Next, the temperature was rapidly increased to 37 °C (2) and, at the indicated time (ranging from 0 to 80 min), cell culture supernatants were replaced by media containing NH₄Cl to increase the pH and block viral fusion (3). Cells were collected at 16 h post-infection and subsequently analysed by immunostaining (with antisera raised against TOSV) and

flow cytometry (4). Figure panel created with BioRender. THIESSON, A. (2025) <https://BioRender.com/m49c678> **(B)** The graphic shows the percentages of TOSV-infected cells normalized to those incubated at 37 °C throughout the experiment (i.e., for 80 min). Penetration kinetics were modelled using a 3-parameter logistic model described elsewhere²⁰ and are represented in the graph as curves. The grey zones indicate the 95% confidence interval. Each experiment was performed in duplicate and at least three times independently. Bars indicate standard deviations.

viral particles was determined by virus titration assays (Fig. 7). As shown in Fig. 7A, rTOSV-B infected cells released more Seg-S and Seg-M than rTOSV-A, even though rTOSV-A produced more infectious viral particles than rTOSV-B (Fig. 7B). To assess the infectivity of the physical viral particles produced by rTOSV-A and rTOSV-B, the ratio of genomic copies

versus the number of infectious viral particles was calculated (Fig. 7C). Our results show that, regardless of the particle segment considered, this ratio is significantly higher for rTOSV-B than rTOSV-A (p -value < 0.01; Fig. 7C), suggesting that rTOSV-A is more efficient at producing infectious virus particles than rTOSV-B.

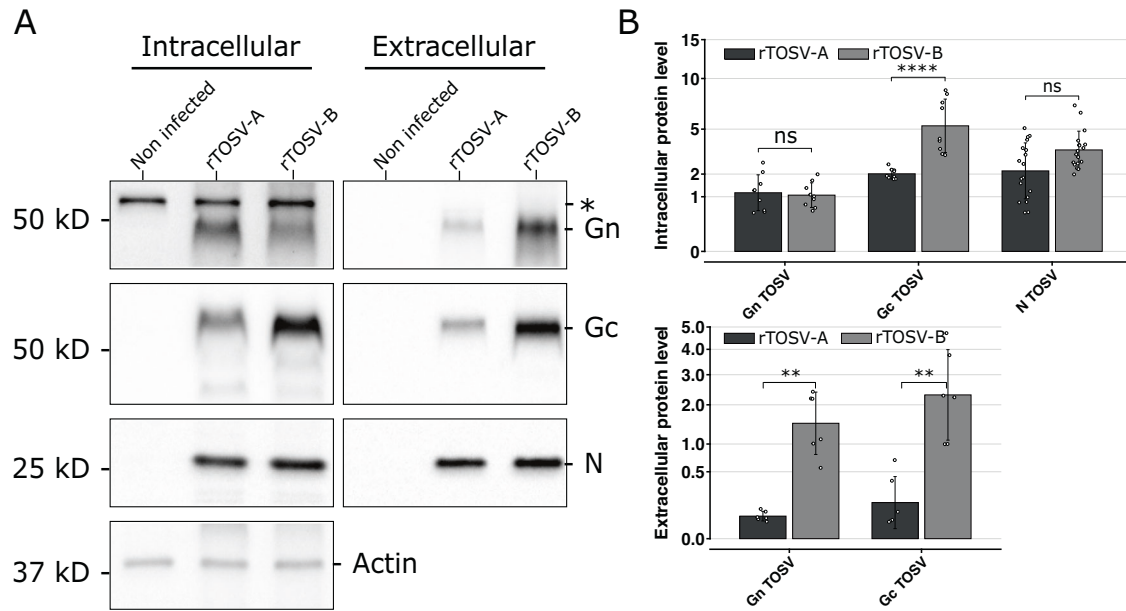


Fig. 6 | Intracellular and extracellular protein levels of rTOSV-A and rTOSV-B Gn and Gc glycoproteins. A Following infection of A549 Npro cells (MOI = 0.1) with rTOSV-A or rTOSV-B viruses, cells and supernatants were collected at 24 h post-infection and analysed by western blot with antisera raised against TOSV N, Gn or Gc proteins, or actin, as indicated. Each experiment was performed in triplicate and at least three times independently. Representative blots are presented. A non-specific band in cell lysates was observed with TOSV Gn antibody and is indicated by

an asterisk. Uncropped blots are supplied in Fig S3. B Signals from rTOSV-A and rTOSV-B N, Gn, Gc, and actin were quantified from three independent experiments using Image Lab software. Protein levels were normalized against actin levels for the intracellular compartment or against N protein level for the extracellular fraction. Bars indicate standard deviations. Statistical significance was determined using multiple Wilcoxon tests with the BY *p*-value adjustment method: *p* > 0.05 (ns: not significant), *p* < 0.01 (**), and *p* < 0.0001 (****).

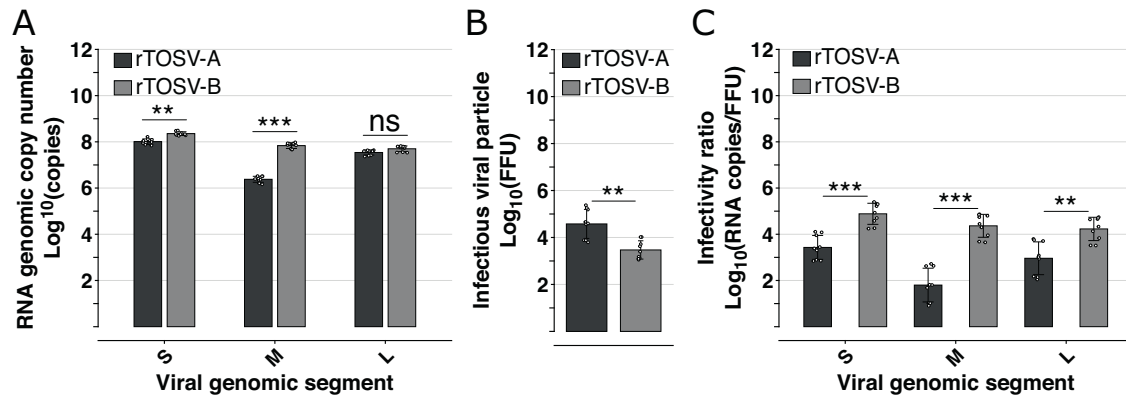


Fig. 7 | rTOSV-A virions are more infectious than rTOSV-B. A549 Npro cells were infected with rTOSV-A or rTOSV-B (MOI = 0.2). Cell culture supernatants were collected at 24 h post-infection, before the appearance of cytopathic effects. A RNA copy numbers of Seg-S, Seg-M, and Seg-L of rTOSV-A and rTOSV-B were quantified by RT-qPCR. B Infectious viral particle number was determined by foci forming assay and expressed as Log₁₀(FFU). C The infectivity of viral particles was

estimated by calculating the ratio of genomic RNA copies against infectious viral titers. Each experiment was performed in triplicate and at least three times independently. Bars indicate standard deviations. Statistical significance was determined using multiple Wilcoxon tests with BY *p*-value adjustment method: *p* > 0.05 (ns: not significant), *p* < 0.01 (**), and *p* < 0.001 (***).

rTOSV-A and rTOSV-B virions differ in size and structure

Finally, the structure of rTOSV-A and rTOSV-B virions was analyzed by transmission electron microscopy. As previously shown for other bunyaviruses²¹, rTOSV-A and rTOSV-B virions were detected within the Golgi apparatus of TOSV-infected cells (Fig. 8A, B). Intriguingly, rTOSV-A and rTOSV-B virions surfaces seemed to be structured differently in the samples from cell supernatants (Fig. 8C). More specifically, the surfaces of rTOSV-B virions appeared to be more structured and organised than those of rTOSV-A virions (Fig. 8C). Furthermore, while no significant difference was observed in the size of intracellular virions, a significant difference of 20 nm was measured between rTOSV-A and rTOSV-B virions in the supernatants of infected cells (*p*-value < 0.0001; Fig. 8D).

Discussion

In this study, we developed a new reverse genetic system for wt TOSV-B to carry out a comparative approach between two genetically distinct TOSV strains. This allowed us to unveil that the genetic diversity of TOSV significantly impacts its biological properties. More specifically, we demonstrated that two TOSV strains belonging to two lineages A and B displayed different replication kinetics in mammalian cell lines. We showed that TOSV-A and TOSV-B have different Gn and Gc coding sequences, and that these sequences contain the determinant(s) responsible for the different viral replication kinetics.

Gn and Gc proteins are key viral proteins involved in phlebovirus entry¹⁹. Indeed, as described by Halldorsson *et al.* for Rift Valley fever virus

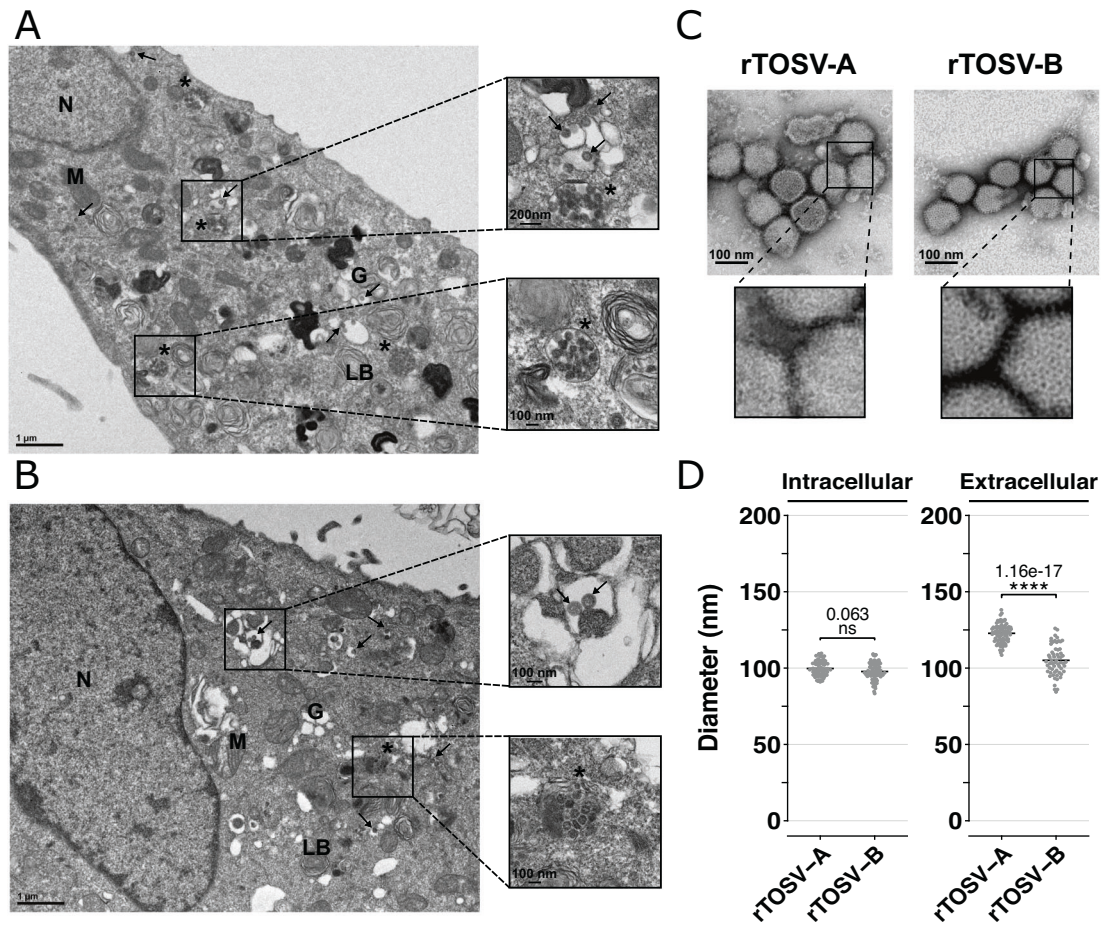


Fig. 8 | rTOSV-A and rTOSV-B virions differs in surface structure and size. A, B A549 Npro cells were infected with rTOSV-A (A) and rTOSV-B (B) viruses (MOI = 0.1). Cells were fixed at 24 h post-infection, before the appearance of cytopathic effects, and prepared for ultrastructural study as described in Materials and Methods. Ultrathin sections of cell pellets were cut, collected on grids, and stained before observations under transmission electron microscope. Representative pictures of rTOSV-A or rTOSV-B infected cells are shown. The experiment was performed in duplicate; at least 15 different infected cells were imaged per condition. Arrows indicate virions present within the Golgi apparatus. Unidentified vesicles

containing electron-dense virus-like structures are indicated with an asterisk. N nucleus, M mitochondria, G Golgi apparatus, LB lamellar body. C rTOSV-A and rTOSV-B virions from cell supernatants were purified, and the viral particles were observed by transmission electron microscopy after negative staining. Representative pictures of rTOSV-A or rTOSV-B virions are shown. D The diameter of viral particles detected inside the cells or in the cell supernatants was determined. At least 60 different virions were analysed per condition. Statistical significance was determined using T-test with BY *p*-value adjustment method: *p* > 0.05 (ns: not significant) and *p* < 0.0001 (****).

(RVFV), Gn mediates the primary cell attachment and prevents early fusion event, while Gc contains the fusion peptide and is therefore responsible for viral membrane fusion in the late endosome²². Along these lines, our results showed that rTOSV-A penetrates cells faster than rTOSV-B. Further analyses on rTOSV-A and rTOSV-B entry, similar to those already performed elsewhere²³, would help us defining more precisely at which step of this process these two TOSV viruses differ.

Importantly, the infectivity of newly produced viral particles was found to be higher for rTOSV-A than rTOSV-B. Due to the segmented nature of bunyavirus genomes, the generation of infectious progeny relies on an efficient genome packaging that is thought to be modulated by the Gn protein^{24,25}. Interestingly, although rTOSV-B displayed higher levels of Gn-Gc proteins and genomic RNA copies than rTOSV-A, it produced lower levels of infectious virus particles. These differences may be due to a less efficient genome packaging process in rTOSV-B than rTOSV-A due to the amino acid differences found in the glycoprotein coding sequences of these two viruses. It has been demonstrated, for example, that RVFV virion production is particularly inefficient in mammalian cell lines, with the vast majority of viral particles lacking one or two viral genomic segments²⁶. Whether the same mechanisms are occurring in TOSV and could explain the differences observed between our two strains remains to be investigated. Moreover, further experiments are needed to identify which amino acid(s)

of the Gn or Gc protein is (are) involved in the differences observed, and to what extent these differences are specific to these two strains or, more generally, to the two genetic lineages.

Interestingly, we observed a difference in the size of Gc and in the amount of Gn and Gc in the supernatants of cells infected with rTOSV-A or rTOSV-B. The reason for the different molecular weight of Gc proteins is not yet known, though it would appear unrelated to N-glycosylation. One can speculate that these two proteins are cleaved differently: a longer rTOSV-A Gc or a shorter rTOSV-B Gc protein could in turn affect their folding and interaction with Gn, resulting, respectively, in reduced or increased glycoprotein incorporation on the surface of viral particles, and/or in morphological changes of the virions. Differences in amino acids and protein folding may also impact protein stability, which could explain why less Gc was detected in rTOSV-A-infected cells compared to rTOSV-B. Since Gn and Gc are translated in the endoplasmic reticulum, they are particularly susceptible to the unfolded-protein response (UPR)²⁷. A quantitative study of the UPR induced by infection, similar to what was done for Severe Fever with Thrombocytopenia Syndrome virus²⁸, would help clarify this point.

Additionally, a lower level of Gn-Gc incorporation in rTOSV-A particles compared to rTOSV-B may result in a more relaxed virion structure, explaining the larger size and rougher/more irregular surface of rTOSV-A

compared to rTOSV-B virions. Lastly, the amount of viral glycoproteins incorporated at the surface of virus particles can affect virus entry, as shown for RVFV, where higher incorporation of the p78 glycoprotein results in reduced replicative capacity and lower virus binding to the cell surface, ultimately leading to inefficient virus internalisation²⁹.

The difference in virion surface structure could also be related to pH sensitivity. Indeed, studies on Uukuniemi and La Crosse viruses have shown that pH can affect virion structure, leading to two distinct spike conformations^{30,31}, which are relatively similar to the differences observed between rTOSV-A and rTOSV-B. This could also correlate with the faster internalization process observed for rTOSV-A, as a conformational change occurring at a higher pH in the endosome could lead to an earlier fusion event compared to rTOSV-B. Thus far, no high-resolution structure of TOSV particles has yet been described, making it impossible to predict how much the sequence diversity between Gn and Gc of TOSV-A and TOSV-B could affect virion structure and pH sensitivity. Further investigations using high-resolution cryo-electron microscopy would be required to analyse these differences.

Although no inter-lineage reassortant viruses have yet been reported for TOSV, their existence was described for numerous species belonging to the *Bunyavirales*³². These events can lead to the emergence of new public-health threatening agents, like the Ngari virus in Africa³³, and are therefore of particular importance for surveillance. In this study, we showed that all segment combinations resulted in efficient virus rescue in vitro. It, therefore, appears that reassortment between TOSV-A and TOSV-B is possible in nature, especially given that these two TOSV strains and lineages are co-circulating in France^{15,16}. Importantly, the vast majority of reassortments described for *Bunyavirales* to date involve the exchange of the Seg-M³⁴, and we identified this segment as a key element in modulating infection by the two TOSV strains studied. Hence, TOSV reassortment, especially those involving Seg-M, should be monitored more closely as such an event may significantly alter the biology of the virus in terms of pathogenicity. The characterisation of circulating TOSV strains by sequencing is therefore important and represents a challenge for the surveillance of this virus. Comparative approaches between different strains of TOSV, such as those carried out in this study, are thus crucial to determine to what extent and how the genetic diversity of TOSV influences its biology. Moreover, the data gathered from this kind of approaches may be relevant to better characterize the pathogenicity of the disease and develop vaccine strategies taking into account TOSV glycoproteins genetic diversity.

Materials and Methods

Cells

BSR, BSR T7/5 CL21, VeroE6, A549 and A549 Npro and A549V cells were grown in Dulbecco's Modified Eagle Medium (DMEM) (Gibco, Thermo Fisher Scientific, France), supplemented with 10% heat-inactivated foetal bovine serum (FBS) (GE HEALTHCARE Europe GmbH, Germany). All cell lines were cultured in a 37 °C, 5% CO₂ humidified incubator. BSR cells are derived from the BHK-21 cells and were kindly provided by Karl-Klaus Conzelmann (Ludwig-Maximilians-University Munich, Gene Center, Munich/Germany). BSR T7/5 CL21 cells are a clone from the BSR T7/5 cell line³⁵. VeroE6 cells were obtained from Philippe Marianneau (Unité de virologie - ANSES Lyon, France). A549 Npro and A549V cells were obtained from Richard E. Randall (University of St. Andrews, UK). A549 Npro cells are derived from the A549 cell line and are constitutively expressing the N protein of the bovine viral diarrhoea virus that blocks the interferon synthesis pathway¹⁷. In A549V cells, stimulation by IFN-I is inhibited by the expression of the V protein of the simian virus 5³⁶.

Production of rTOSV-B reverse genetic plasmids

Viral RNA was extracted from TOSV MRS2010-4319501 (wt TOSV-B)¹⁶ (obtained from EVAg, France) BSR infected cells using Trizol reagent (Thermo Fisher Scientific, France) following the manufacturer's protocol. RNA was then purified using the RNeasy Plus Mini kit (QIAGEN,

Germany). Complementary DNA (cDNA) was synthesized using Omniscript RT polymerase (QIAGEN, Germany) and viral genomic segment-specific primers. Primers and viral RNAs were first incubated for 10 min at 65 °C before the RT reaction following manufacturer protocol. Full-length segments were then amplified from cDNA by PCR using CloneAmp HIFI PCR Premix (Takara, France) and then gel purified using NucleoSpin Gel and PCR Clean-up kit (Macherey-Nagel, Germany). The plasmid backbone, containing the T7 promoter and terminator, the HDV ribozyme and the ampicillin resistance gene, was amplified by PCR from the pUC57 plasmid used in the TOSV reverse genetic system described previously¹³. Linearized plasmids were digested for 1 h at 37 °C by DpnI (New England Biolabs, UK) prior to performing the cloning reaction using the In-Fusion HD-Cloning Plus kit (Takara, France) according to the manufacturer's instruction with a molar ratio insert:vector of 2:1 for the S and M segment and a 1:2 molar ratio for the L segment. Stellar competent bacteria (Takara, France) were used for transformation and plasmid amplification following manufacturer protocol. To construct chimeric plasmids, the NSm or Gn-Gc coding sequences were amplified by PCR from the reverse genetic plasmid of TOSV-A or -B. Additionally, pUC57-TOSV_M-ΔNSm or -ΔGn-Gc plasmids were generated by PCR on plasmids pUC57-TOSV-A_M or pUC57-TOSV-B_M. Chimeric plasmids were then ligated and amplified using In-Fusion cloning process as described above. The sequences of all generated plasmids were verified by sequencing. All RT and PCR primer sequences are available on request.

Validation of the plasmid's sequences

After sequencing, plasmid sequences were compared to wt TOSV-B strain and other lineage B TOSV strains (TOSV/P51: KU204978-KU204980, TOSV 9028: KU904263-KU904265, TOSV 11368: KU925897-KU925899, TOSV 54441132704: KX010932-KX010934, TOSV P233: KU204975-KU204977, TOSV H4906: KU922125-KU922127, TOSV 5963930705: KU935733-KU935735, and TOSV Nice/113: KU204981-KU204983) using MUSCLE software³⁷. For each nucleotide substitution in comparison to the deposited sequence of wt TOSV-B, RNA was extracted from the viral stock, the region concerned was amplified by RT-PCR, and then sequenced.

Rapid amplification of cDNA-ends by polymerase chain reaction (RACE-PCR)

The genome and antigenome 3' termini were sequenced using RACE-PCR analysis as described before¹³. Briefly, RNA was extracted from viral stock using QIAmp viral RNA (QIAGEN, Germany), polyadenylated with *E. coli* Poly(A) Polymerase I from mMACHINE™ T7 ULTRA kit (Invitrogen, by Life Technologies, Thermo Fisher Scientific, France) before being purified using RNeasy® Plus Mini kit (QIAGEN, Germany). Complementary DNA was synthesized using the PrimeScript RT reagent kit (Takara, France) and oligo-d(T)-AP primer (GACCACGCGTATCG ATGTCGACTTTTTTTTTT). Seg-S termini were then amplified using anchor primer (GACCACGCGTATCGATGTCGAC) and RACE_-TOSV_S1 (CCACCTCATTAGCCTGCTTAG) or RACE_TOSV_S2 (GTCACCTCTTGTCTTCCTTAG). Seg-M termini were amplified using anchor primer and RACE_TOSV_M1 (TTCTCTTCCGTTCCAGCTC) or RACE_TOSV_M2 (CCATATTCTCCAGAGCCTCG). Seg-L termini were amplified using anchor primer and RACE_TOSV_L1 (TCCTCA GTCTGCTGACAGTC) or RACE_TOSV_L2 (TCCTGACTCAGAGCCT GAAG). Sequences were next determined using Sanger sequencing. Site-directed mutagenesis was performed on the 3' antigenomic terminus of the Seg-S and the 5' antigenomic terminus of Seg-L in order to align plasmid sequences with those obtained from the RACE-PCR analysis. Briefly, after a 12-cycle PCR, PCR products were treated with DpnI and purified on agarose gel. Plasmids were then transformed and amplified as described above, and the plasmid sequences were reassessed by Sanger sequencing. Complete sequences of each segment used for the reverse genetics system (Seg-L, Seg-M and Seg-S) are accessible under the GenBank accession numbers PQ015116, PQ015117 and PQ015118, respectively.

Virus production by reverse genetics

Viral rescue was carried out by transfection using Lipofectamine 2000 (Invitrogen by Life Technologies, Thermo Fisher Scientific, France). BSR T7/5 CL21 cells were seeded in six-well plates at a density of 3×10^5 cells per well and incubated for 24 h to reach 80% of confluency. Culture media was changed to 1 mL of DMEM complemented with 4% of FBS. Cells were then transfected with 500 ng of each plasmid expressing the S, M and L RNA antigenome under the control of a T7 RNA polymerase promoter by using 3 μ L of Lipofectamine 2000 in a final volume of 60 μ L of OptiMEM (Gibco, Thermo Fisher Scientific, France). After incubation for 6 h at 37 °C and 5% CO₂, cells were washed with 1 mL of phosphate-buffered saline (PBS; Sigma-Aldrich, Merck, France). Then, 2 mL of DMEM supplemented with 4% FBS was added to each well, and the cells were further incubated at 37 °C until cytopathic effects appeared. The cell supernatants, referred to as passage 0 (p0), were then collected, clarified by centrifugation and stored at -80 °C.

Viral stock production

All viral stocks were amplified from p0 on VeroE6 cells for 2 to 3 days in DMEM supplemented with 4% FBS at 37 °C and 5% CO₂. For high MOI infection assays, viral stocks were concentrated by ultracentrifugation. Briefly, VeroE6 were seeded 3 days prior to infection using p0. Four days later, media was collected and clarified by centrifugation before ultracentrifugation on a 20% (g/mL) ultrapure sucrose diluted in PBS (Invitrogen by Life Technologies, Thermo Fisher Scientific, France). Ultracentrifugation was performed in an Optima XE-90 machine (Beckman Coulter Life Sciences, USA) at 124,000 g for 3 h at 4 °C. Pellets were then resuspended in PBS and stored at -80 °C.

Foci forming titration assays

Viral stock titers were determined by foci-forming assays using VeroE6 cells. Briefly, VeroE6 cells seeded in 12-well plates were infected with 10-fold serial dilutions of virus stocks and incubated for 2 h at 37 °C. The media was then removed and wash twice in PBS. Cells were then covered with 1.5 mL of a semisolid overlay containing a volume-to-volume mixture of 2.5% ultrapure agarose (Life Technologies, Thermo Fisher Scientific, France) and 2X minimal essential medium (MEM; Gibco, Thermo Fisher Scientific, Villebon-sur-Yvette, France) supplemented with 4% FBS and incubated at 37 °C for 6 days. Cells were then fixed in 4% formaldehyde (Fisher Chemical, Thermo Fisher Scientific, USA) overnight at 4 °C, before agarose overlay removal and permeabilization with 0.1% Triton (Euromedex, France) in PBS. A first blocking step was performed with a solution consisting of PBS containing 0.1% Tween 20 (Euromedex, France) and 0.4% gelatine fish (Sigma-Aldrich, Merck, Germany), prior to a second blocking using a solution with 0.1% Tween 20 and 2.5% FBS in PBS. Cells were then incubated overnight at 4 °C and under agitation with mouse ascites raised against TOSV (1:2500 in second blocking solution) kindly supplied by Philippe Marianneau (Unité de virologie, ANSES Lyon, France). Infection foci were visualised using the appropriate secondary antibody coupled with horseradish peroxidase (HRP; 1:5000, Sheep Anti-Mouse IgG A5906, Sigma-Aldrich, Merck, Germany) and TrueBlue™ chemical (SeraCare, LGC Clinical Diagnostics, USA). Infection foci were then counted to determine the viral titer expressed as FFU/mL (Foci Forming Unit).

In vitro growth curves

Monolayer of A549 or A549 Npro cells were seeded 24 h before infection in 12-well plates (2.5×10^5 cells per well). Cells were then incubated at 37 °C and 5% CO₂ with the different viruses at a multiplicity of infection (MOI) of 0.01 in DMEM complemented with 4% FBS. After two hours of infection, cells were washed twice in PBS and further incubated at 37 °C in DMEM 4% FBS. At 24-, 48- and 72-hours post-infection, 100 μ L of the cell supernatants were collected for viral titration by limiting dilution assays in A549V cells. A549 V cells were chosen for this assay to accurately assess viral titers without interference from IFN-I potentially present in the supernatant of infected A549 cells, as these cells are unresponsive to IFN-I. Briefly, in a 96-

well plate, 11 μ L of cell supernatants were diluted in quadruplicate by a 10-fold serial dilution (from 10^{-1} to 10^{-12}) in 100 μ L of DMEM supplemented with 4% FBS. Then, 4×10^3 A549V cells were added to each well and incubated for 6 days at 37 °C in 5% CO₂. Cytopathic effects were assessed under a microscope, and viral titers were expressed as 50% tissue culture infective doses (TCID₅₀/mL) using the Reed and Muench method³⁸. Growth curve experiments were stopped at 72 h post-infection, as significant cytopathic effects were starting to appear. Each experiment was done in triplicate and repeated at least three times independently, using two independent viral stocks. For each experiment, initial viral inocula were titrated using a foci-forming assay to ensure that all viral infections started with equal input levels. Additionally, a post-washing control time point was included and titrated by limiting dilution assays to assess the amount of viral material remaining.

Virus entry kinetic

A549 Npro cells were seeded 24 h post-infection in 48-well plates (7.5×10^4 cells per well). Cells were first incubated for 10 min on ice in cold DMEM supplemented with 10% FBS and 20 mM HEPES buffer (Gibco, Thermo Fisher Scientific, USA). rTOSV-A or rTOSV-B infectious viral particles (ranging from 7.5×10^4 to 15×10^4) were bound to the cells on ice for 1 h in cold DMEM supplemented with 0.2% FBS and 20 mM HEPES buffer to synchronise the virus attachment. Then, the cell supernatants were replaced by warm DMEM medium supplemented with 4% FBS and 20 mM HEPES buffer to trigger virus internalisation. At specific times after the temperature shift, the culture medium was replaced with warm DMEM supplemented with 10% FBS, 20 mM HEPES buffer and 50 mM ammonium chloride (NH₄Cl, Merck, Germany). The addition of this weak base results in a rapid increase in pH within the cell³⁹, which inhibits the TOSV acidification-dependent fusion process in endosomes²³. At 16 h post-infection, the medium was removed, and the cells were collected and fixed with a 4% paraformaldehyde solution (PFA, ChemCruz, Santa Cruz Biotechnology, Germany). The percentage of infected cells was determined by flow cytometry. To this end, fixed samples were permeabilised with a solution of PBS containing 0.1% Saponin (Sigma-Aldrich, Merck, Germany) and 10% FBS. Cells were then labelled with mouse ascites directed against TOSV (1/1000) followed by a secondary antibody directed against mouse antibodies coupled to the Alexa-488 fluorochrome (1/1000, A-11001, Invitrogen by Life Technologies, Thermo Fisher Scientific, France). Primary antibodies were incubated for 2.5 h at 37 °C. Secondary antibodies were incubated for 1 h at 37 °C. All antibody solutions were diluted in PBS 0.1% saponin 10% FBS. Cells were then analysed using the Canto II cytometer (Becton Dickinson BD, USA). Data acquisition and analysis were performed using BD FACSDiva™ software (version 6, Becton Dickinson BD, USA). Each experiment was done in duplicate and repeated three times independently, using two independent viral stocks. The virus penetration kinetics were then determined using a 3-parameter logistic model as described by Fontaine et al.²⁰. Model parameters were estimated for each condition using a non-linear least squares method based on the Gauss-Newton algorithm. Modelling was carried out using R (version 4.2.3) and R Studio (version 2023.03.0 + 386).

Western blotting

A549 Npro cells were infected at an MOI of 0.1 with rTOSV-A or rTOSV-B viruses. At 2 h post-infection, the cells were washed successively with PBS and DMEM culture medium supplemented with 4% FBS before further incubation at 37 °C and 5% CO₂. At 24 h post-infection, culture media was ultra-centrifuged as described above and the viral pellet was resuspended in Laemmli buffer (Alfa Aesar, Thermo Fisher Scientific, USA) diluted in PBS. Cells were then washed once in PBS and lysed using Laemmli buffer. Extracellular and intracellular cell lysates were heated at 90 °C for 10 min and stored at -20 °C. Proteins were separated by SDS-PAGE on 10% polyacrylamide gel and transferred to nitrocellulose membranes (Trans Blot Turbo RTA transfer kit midi, BioRad, Marnes-La-Coquette, France). Membranes were blocked in tris buffer saline (TBS) with 0.1% Tween and

5% dry milk (Euromedex, Souffelweyersheim, France) solution, then incubated overnight at 4 °C with a polyclonal guinea pig primary antibody against TOSV Gn (1:1000)¹⁴, a polyclonal guinea pig antibody against TOSV Gc (1:2000)¹⁴, or a mouse ascites raised against TOSV (1:2500). Anti-TOSV hyperimmune mouse ascitic fluid was obtained as previously described for RVFV⁴⁰. BALB/c mice were inoculated intraperitoneally with inactivated TOSV-infected mouse brain suspensions in Freund's complete adjuvant on day 0 and 1 and in Freund's incomplete adjuvant on day 7 and 14. On day 21 and 28, mice were inoculated with virulent suspension in Freund's incomplete adjuvant. Finally, the mice were inoculated intraperitoneally with TG180 sarcoma cells on day 25. One week later, ascitic fluid was harvested and stored at -80 °C until use. Actin was detected with monoclonal mouse antibody coupled with horseradish peroxidase (HRP; 1:75,000; A3854, Sigma-Aldrich, Merck, Saint-Quentin Fallavier, France). Membranes were exposed to the appropriate peroxidase-conjugated secondary antibodies (1:5000 goat anti-guineapig IgG A108P or 1:10000 sheep anti-mouse IgG A5906; Sigma-Aldrich, MERCK) for 1.5 h and bands were visualized by chemiluminescence using the Clarity ECL Western blotting substrate (BioRad) and ChemiDoc XRS+ System (BioRad). Band intensity was quantified using Image Lab software (Bio-Rad). Each experiment was done in triplicate and repeated three times independently, using two independent viral stocks.

Genome quantification by RT-qPCR

A549 Npro cells were infected at an MOI of 0.2 with rTOSV-A or rTOSV-B viruses as described above for western blotting. At 24 h post-infection, culture media were collected. Part of the cell supernatants was stored at -80 °C for FFU titration assays. For TOSV genome quantification, extracellular RNAs were extracted from the cell supernatants using the QIAmp viral RNA kit (QIAGEN, Germany). Infected cells were lysed in RLT plus buffer (QIAGEN, Germany), and RNAs were extracted using the RNeasy Plus Mini kit (QIAGEN, Germany). RT reactions were performed using the PrimeScript™ RT kit (Takara, France) and the following primers: TOSV_RT_S (ACACAGAGATCCCGTGTATTAATC) for Seg-S, TOSV_RT_M (AGTCCATCCCAAGCACAA) for Seg-M and TOSV_RT_L (CTGGCAAGGGAYATCTTTGA) for Seg-L. The previously published primers STOS-50F and STOS-138R⁴¹ were used for qPCR on Seg-S. Primers MTOS-F (CATWGAGCAGATGAAGATGAG) and MTOS-R (AGCACTTAGAGGCTGATGATG) or LTOS-F (GAT TGAGAGAGAYAGTCTCTACAC) and LTOS-R (GAACTCATAACTC ATCATCTCTGC) were used for quantification of Seg-M and Seg-L respectively. The qPCR reactions were performed using the TBGreen Takara SYBR qPCR kit (Takara, France) following the manufacturer's protocols. A viral genomic RNA standard for each rTOSV-A or rTOSV-B Seg-S, M and L was produced using the T7 RiboMAX™ kit (Promega, France) and a PCR template containing a T7 promoter amplified from each reverse genetic plasmid. DNA contaminants were removed using the TURBO DNA-free™ kit (Invitrogen by Life Technologies, Thermo Fisher Scientific, France). Each experiment was done in triplicate and repeated at least three times independently, using two independent viral stocks.

Transmission electron microscopy

A549 Npro cells were infected in a 6-well plate at an MOI of 0.1 in duplicate, as described before. At 24 h post-infection, infected cells were fixed with 2% glutaraldehyde (Electron Microscopy Science, USA) in 0.1 M sodium cacodylate buffer (pH 7.4) at room temperature for 30 min. After three washes in 0.2 M sodium cacodylate buffer, cells were post-fixed with 1% osmium tetroxide (Electron Microscopy Science, USA) at room temperature for 1 h, dehydrated in a graded series of ethanol and embedded in Epon. After polymerization, ultrathin sections (100 nm) in 0.15 M sodium cacodylate (pH 7.4) buffer were cut using an ultramicrotome UCT (Leica Microsystems, France) and collected on 200 mesh grids. Sections were stained with uranyl acetate and lead citrate before observations on a 1400JEM transmission electron microscope (JEOL, Japan) equipped with an Oriem camera and Digital Micrograph. For extracellular virions analysis,

FBS and PBS were first ultra-centrifugated at 100000 g for 18 h before filtration (0.2 µm) to prepare exo-free FBS and ultrapure PBS. A549 Npro cells were seeded in 175 cm² culture flasks (1 × 10⁷ cells per flask) 24 h before infection with rTOSV-A or rTOSV-B which were diluted in DMEM supplemented with 4% exo-free FBS. Four days later, the cell supernatants were collected and clarified by successive centrifugation and filtration (2000g for 20 min, 5250 g for 30 min, and filtration with a 0.45 µm filter followed by a further filtration with a 0.2 µm filter). Clarified cell supernatant was then fixed with 2% PFA (10 mL of 8% EM grade PFA, Electron Microscopy Science, USA). The fixed viral particles were then purified by ultra-centrifugation at 124,000 g for 2 h, resuspended in 30 mL of ultrapure PBS and ultra-centrifugated a second time as described above. The pellets were then resuspended in ultrapure PBS and adsorbed on 200 mesh nickel grids coated with formvar-C for 2 min at RT. Then, grids were coloured with 2% phosphotungstic acid for 2 min and observed with the transmission electron microscope described before. Virion diameters were measured using Fiji software⁴², and their size in nm was calculated by setting the software pixel/mm ratio on the scale of each image.

Statistical analysis

Statistical analyses were performed using R and RStudio software and the rstatix package (<https://CRAN.R-project.org/package=rstatix>). If data followed a normal distribution, the ANOVA test was first used with a significance threshold of 0.01. Multiple T-tests with p-value adjustment⁴³ were used as follow-up tests. If not, the Kruskal-Wallis test was first used with a significance threshold of 0.01. In case of statistical significance, data were then compared between conditions using multiple Wilcoxon-Mann-Whitney tests as a follow-up test with Benjamini-Yekutieli (BY) p-value adjustment. Graphical representation was realized using ggplot2 package (<https://CRAN.R-project.org/package=ggplot2>).

Data availability

Data is provided within the manuscript or supplementary information files. Complete sequences of each TOSV segment used for the reverse genetics are accessible under the GenBank accession numbers: PQ015116, PQ015117 and PQ015118.

Received: 13 September 2024; Accepted: 31 March 2025;

Published online: 15 April 2025

References

- Depaquit, J., Grandadam, M., Fouque, F., Andry, P. E. & Peyrefitte, C. Arthropod-borne viruses transmitted by Phlebotomine sandflies in Europe: a review. *Euro Surveill.* **15**, 19507 (2010).
- Verani, P. et al. Ecological and epidemiological studies of Toscana virus, an arbovirus isolated from Phlebotomus. *Ann Ist Super Sanita.* **18**, 397–399 (1982).
- Dersch, R. et al. Toscana virus encephalitis in Southwest Germany: a retrospective study. *BMC Neurol.* **21**, 495 (2021).
- Al-Numaani, S. A. et al. Seroprevalence of Toscana and sandfly fever Sicilian viruses in humans and livestock animals from western Saudi Arabia. *One Health.* **17**, 100601 (2023).
- Ayhan, N., Eldin, C. & Charrel, R. Toscana virus: A comprehensive review of 1381 cases showing an emerging threat in the Mediterranean regions. *J Infect.* **90**, 106415 (2025).
- Braitto, A. et al. Evidence of Toscana virus infections without central nervous system involvement: a serological study. *Eur J Epidemiol.* **13**, 761–764 (1997).
- Baldelli, F. et al. Unusual presentation of life-threatening Toscana virus meningoencephalitis. *Clin Infect Dis.* **38**, 515–520 (2004).
- Dupouey, J. et al. Toscana virus infections: A case series from France. *J Infect.* **68**, 290–295 (2014).
- Ayhan, N. & Charrel, R. N. An update on Toscana virus distribution, genetics, medical and diagnostic aspects. *Clin Microbiol Infect.* <https://doi.org/10.1016/j.cmi.2019.12.015> (2020).

10. Ayhan, N., Prudhomme, J., Laroche, L., Bañuls, A.-L. & Charrel, R. N. Broader Geographical Distribution of Toscana Virus in the Mediterranean Region Suggests the Existence of Larger Varieties of Sand Fly Vectors. *Microorganisms*. **8**, E114 (2020).
11. Punda-Polić, V. et al. Evidence of an autochthonous Toscana virus strain in Croatia. *J Clin Virol*. **55**, 4–7 (2012).
12. Papa, A. et al. Severe encephalitis caused by Toscana virus, Greece. *Emerg Infect Dis*. **20**, 1417–1419 (2014).
13. Alexander, A. J. T. et al. Development of a Reverse Genetics System for Toscana Virus (Lineage A). *Viruses*. **12**, (2020). <https://doi.org/10.3390/v12040411>
14. Woelfl, F. et al. Novel Toscana Virus Reverse Genetics System Establishes NSs as an Antagonist of Type I Interferon Responses. *Viruses*. **12**, E400 (2020).
15. Charrel, R. N. et al. Cocirculation of 2 genotypes of Toscana virus, southeastern France. *Emerg Infect Dis*. **13**, 465–468 (2007).
16. Nougairede, A. et al. Isolation of Toscana virus from the cerebrospinal fluid of a man with meningitis in Marseille, France, 2010. *Vector Borne Zoonotic Dis*. **13**, 685–688 (2013).
17. Hilton, L. et al. The NPro product of bovine viral diarrhea virus inhibits DNA binding by interferon regulatory factor 3 and targets it for proteasomal degradation. *J Virol*. **80**, 11723–11732 (2006).
18. Grò, M. C., Di Bonito, P., Fortini, D., Mochi, S. & Giorgi, C. Completion of molecular characterization of Toscana phlebovirus genome: nucleotide sequence, coding strategy of M genomic segment and its amino acid sequence comparison to other phleboviruses. *Virus Res*. **51**, 81–91 (1997).
19. Spiegel, M., Plegge, T. & Pöhlmann, S. The Role of Phlebovirus Glycoproteins in Viral Entry, Assembly and Release. *Viruses*. **8**, 202 (2016).
20. Fontaine, A. et al. Epidemiological significance of dengue virus genetic variation in mosquito infection dynamics. *PLoS Pathog*. **14**, e1007187 (2018).
21. Barker, J., daSilva, L. L. P. & Crump, C. M. Mechanisms of bunyavirus morphogenesis and egress. *J. Gen. Virol*. **104**, (2023). <https://doi.org/10.1099/jgv.0.001845>
22. Halldorsson, S. et al. Shielding and activation of a viral membrane fusion protein. *Nat Commun*. **9**, 349 (2018).
23. Koch, J. et al. The phenuivirus Toscana virus makes an atypical use of vacuolar acidity to enter host cells. *PLoS Pathog*. **19**, e1011562 (2023).
24. Overby, A. K., Petterson, R. F. & Neve, E. P. A. The glycoprotein cytoplasmic tail of Uukuniemi virus (Bunyaviridae) interacts with ribonucleoproteins and is critical for genome packaging. *J Virol*. **81**, 3198–3205 (2007).
25. Carnec, X., Ermonval, M., Kreher, F., Flamand, M. & Bouloy, M. Role of the cytosolic tails of Rift Valley fever virus envelope glycoproteins in viral morphogenesis. *Virology*. **448**, 1–14 (2014).
26. Wichgers Schreur, P. J. & Kortekaas, J. Single-Molecule FISH Reveals Non-selective Packaging of Rift Valley Fever Virus Genome Segments. *PLoS Pathog*. **12**, e1005800 (2016).
27. Hetz, C., Zhang, K. & Kaufman, R. J. Mechanisms, regulation and functions of the unfolded protein response. *Nat Rev Mol Cell Biol*. **21**, 421–438 (2020).
28. Zhang, L.-K. et al. Quantitative Proteomic Analysis Reveals Unfolded-Protein Response Involved in Severe Fever with Thrombocytopenia Syndrome Virus Infection. *J Virol*. **93**, e00308–e00319 (2019).
29. Terasaki, K. et al. Rift Valley fever virus 78kDa envelope protein attenuates virus replication in macrophage-derived cell lines and viral virulence in mice. *PLoS Negl Trop Dis*. **15**, e0009785 (2021).
30. Wang, G. J., Hewlett, M. & Chiu, W. Structural variation of La Crosse virions under different chemical and physical conditions. *Virology*. **184**, 455–459 (1991).
31. Overby, A. K., Petterson, R. F., Grünewald, K. & Huisken, J. T. Insights into bunyavirus architecture from electron cryotomography of Uukuniemi virus. *Proc Natl Acad Sci USA*. **105**, 2375–2379 (2008).
32. Briese, T., Calisher, C. H. & Higgs, S. Viruses of the family Bunyviridae: are all available isolates reassortants?. *Virology*. **446**, 207–216 (2013).
33. Gerrard, S. R., Li, L., Barrett, A. D. & Nichol, S. T. Ngari virus is a Bunyamwera virus reassortant that can be associated with large outbreaks of hemorrhagic fever in Africa. *J Virol*. **78**, 8922–8926 (2004).
34. Kapuscinski, M. L. et al. Genomic characterization of 99 viruses from the bunyavirus families Nairoviridae, Peribunyaviridae, and Phenuiviridae, including 35 previously unsequenced viruses. *PLoS Pathog*. **17**, e1009315 (2021).
35. Mottram, T. J. et al. Mutational analysis of Rift Valley fever phlebovirus nucleocapsid protein indicates novel conserved, functional amino acids. *PLoS Negl Trop Dis*. **11**, e0006155 (2017).
36. Didcock, L., Young, D. F., Goodbourn, S. & Randall, R. E. The V protein of simian virus 5 inhibits interferon signalling by targeting STAT1 for proteasome-mediated degradation. *J Virol*. **73**, 9928–9933 (1999).
37. Edgar, R. C. MUSCLE: multiple sequence alignment with high accuracy and high throughput. *Nucleic Acids Res*. **32**, 1792–1797 (2004).
38. Lindenbach, B. D. Measuring HCV infectivity produced in cell culture and in vivo. *Methods Mol Biol*. **510**, 329–336 (2009).
39. Ohkuma, S. & Poole, B. Fluorescence probe measurement of the intralysosomal pH in living cells and the perturbation of pH by various agents. *Proc Natl Acad Sci USA*. **75**, 3327–3331 (1978).
40. Chrun, T. et al. A Rift Valley fever virus Gn ectodomain-based DNA vaccine induces a partial protection not improved by APC targeting. *NPJ Vaccines*. **3**, 14 (2018).
41. Pérez-Ruiz, M., Collao, X., Navarro-Marí, J.-M. & Tenorio, A. Reversetranscription, real-time PCR assay for detection of Toscana virus. *J Clin Virol*. **39**, 276–281 (2007).
42. Schindelin, J. et al. Fiji: an open-source platform for biological-image analysis. *Nat Methods*. **9**, 676–682 (2012).
43. Benjamini, Y. & Yekutieli, D. The control of the false discovery rate in multiple testing under dependency. *Ann Stat*. **29**, 1165–1188 (2001).

Acknowledgements

This study was supported by the Institut National de la Recherche pour l'agriculture, l'alimentation et l'environnement, the Ecole Pratique des Hautes Etudes and the University of Lyon 1. A.T. was a doctoral fellow of the École Doctorale de l'École Pratique des Hautes Études (ED472). A.K. was supported by UK Medical Research Council MC_UU_12014/8, and MC_UU_00034/4. We acknowledge the contribution of the flow cytometry platforms of SFR BioSciences Gerland Lyon Sud (UMS3444/US8) and SFR Santé Lyon-Est (UAR3453 CNRS, US7 Inserm, UCBL) facility: CIQLE (a LyMIC member), especially Elisabeth Errazuriz-Cerda for her help in sample preparation and image acquisition for transmission EM. TOSV strain MRS2010-4319501 was obtained from the European Virus Archive Global (EVAg) project that has received funding from the European Union's Horizon 2020 research and innovation program under grant agreement No 653316. The funders had no role in study design, data collection and analysis, decision to publish, or preparation of the manuscript. We thank Pierre-Yves Lozach (IVPC UMR754, INRAE) and Philippe Marianneau (ANSES Lyon, France) for kindly providing us with TOSV antibodies and useful discussion. We also thank Karl-Klaus Conzelmann and Richard E. Randall for providing us with cells. Finally, we thank Alessia Armezzani for revising the manuscript, and members of our laboratories for useful suggestions.

Author contributions

A.T., M.-P.C., and S.D. performed the experiments. A.T., A.K., F.A., and M.R. designed experiments and analysed the data. A.T. performed the statistical tests and prepared all the figures. A.T., F.A. and M.R. wrote the original draft. All authors corrected the final manuscript.

Competing interests

The authors declare no competing interests.

Additional information

Supplementary information The online version contains supplementary material available at

<https://doi.org/10.1038/s44298-025-00113-0>.

Correspondence and requests for materials should be addressed to Frédérick Arnaud or Maxime Ratinier.

Reprints and permissions information is available at <http://www.nature.com/reprints>

Publisher's note Springer Nature remains neutral with regard to jurisdictional claims in published maps and institutional affiliations.

Open Access This article is licensed under a Creative Commons Attribution 4.0 International License, which permits use, sharing, adaptation, distribution and reproduction in any medium or format, as long as you give appropriate credit to the original author(s) and the source, provide a link to the Creative Commons licence, and indicate if changes were made. The images or other third party material in this article are included in the article's Creative Commons licence, unless indicated otherwise in a credit line to the material. If material is not included in the article's Creative Commons licence and your intended use is not permitted by statutory regulation or exceeds the permitted use, you will need to obtain permission directly from the copyright holder. To view a copy of this licence, visit <http://creativecommons.org/licenses/by/4.0/>.

© The Author(s) 2025